ACS Sustainable Chemistry & Engineering

Research Article

Cite This: ACS Sustainable Chem. Eng. 2019, 7, 5240−5248

pubs.acs.org/journal/ascecg

Nitrogen-Doped Carbon Polyhedra Nanopapers: An Advanced Binder-Free Electrode for High-Performance Supercapacitors

Hengyi Lu,[†,‡] Siliang Liu,[†] Youfang Zhang,[†] Yunpeng Huang,[‡] Chao Zhang,*[,†] and Tianxi Liu*[,†,‡]

[†]State Key Laboratory for Modification of Chemical Fibers and Polymer Materials, College of Materials Science and Engineering, Innovation Center for Textile Science and Technology, Donghua University, 2999 North Renmin Road, Shanghai 201620, P. R. China

[‡]State Key Laboratory of Molecular Engineering of Polymers, Department of Macromolecular Science, Fudan University, 220 Handan Road, Shanghai 200433, P. R. China

Supporting Information

ABSTRACT: Metal−organic framework (MOF)-derived nitrogen-doped porous carbon as electrode material for supercapacitors has recently drawn much attention. However, the development of flexible electrodes composed of MOF-derived carbon is still a great challenge. Herein, nitrogen-doped porous carbon polyhedra (NC) derived from zeolitic imidazolate framework-8 (ZIF8) are assembled into flexible nanopapers assisted with reduced graphene oxide (rGO). The resultant NC/rGO nanopaper shows a hierarchical structure of NC nanoparticle-imbedded rGO framework. A uniform dispersion of NC nanoparticles is achieved due to the rGO framework, and meanwhile, the uniform decoration of NC nanoparticles on rGO nanosheets prevents easy restacking of rGO. A conductive rGO framework further accelerates the electron/ion transportation inside the NC/rGO nanopaper. Furthermore, excellent mechanical performance of rGO framework endows high flexibility to the NC/rGO nanopaper. As a result, the NC/rGO nanopaper as a binder-free electrode delivers high specific capacitance of 280 F g^{-1} at 1 A g^{-1}, high capacitance retention after 5000 cycles, and high energy density of 19.45 W h kg^{-1}.

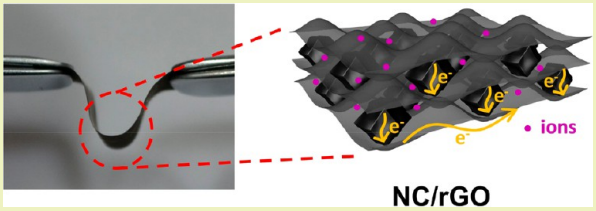

KEYWORDS: *ZIF8, Carbon polyhedron, Reduced graphene oxide, Flexible nanopaper electrode, Supercapacitors*

INTRODUCTION

Metal−organic framework (MOF) is a new type of crystalline porous solids consisting of metal centers with organic linkers via coordination bonds. Recently, MOF-derived materials are regarded as an ideal electrode material for energy storage and conversion applications due to their high surface areas, functional compositions, controllable pore structures, and easy converting features.[1−5] Compared with porous carbon obtained from other organic precursors, MOF-derived carbon usually has tunable porosity and uniformly dispersed nitrogen-doped (N-doped) sites.[6−8] Among various MOFs, zeolitic imidazolate framework-8 (ZIF8), composed of zinc ions and 2-methylimidazole, has been extensively used as the precursor for the synthesis of N-doped porous carbon because of its large pore volume, high nitrogen content, good thermal stability, low cost, etc.[9] Because of their unique structural features, the products of directly pyrolyzed ZIF8 are widely used as electrode materials for supercapacitors.[10]

The typical morphology of ZIF8-derived carbon is polyhedron, which suffers from poor conductivity between individual carbon polyhedra. Besides, the intrinsic aggregation of carbon polyhedra hinders fast mass transport inside the electrode matrix, thereby resulting in poor electrochemical performance. Large efforts are devoted to overcome these drawbacks of ZIF8-derived carbon polyhedra as electrode materials for supercapacitors. Bridging carbon polyhedra by 1D conductive linkers is an effective way to enhance their conductivity.[11−13] For instance, Wan et al. prepared ZIF8-derived carbon/carbon nanotube (CNT) composite electrodes by heterogeneous nucleation and growth of ZIF8 on CNT backbones with subsequent carbonization.[14] The CNT backbones serve as conductive linkers, reducing the resistances between individual carbon polyhedra. In addition to low conductivity between individual carbon polyhedra, the powdery status of ZIF8-derived carbon polyhedra also causes another problem as an electrode, which is inevitably to be mixed with binders, conductive agents, and other additives before being coated on current collectors for the fabrication of electrodes.[15,16] This process is complicated, and the addition of insulating binders will reduce electrical conductivity of electrodes, undoubtedly affecting the electrochemical energy storage performance of the device.[17−20] The development of free-standing electrode greatly simplifies the utilization process of electrode materials.[15,21−24] For example, Lou and co-workers have developed 3D graphene foam (GF)/carbon nanotube (CNT) hybrid films for supporting electroactive materials to construct lightweight and flexible electrodes for high-performance asymmetric supercapacitors.[25] Recently, the

Received: November 26, 2018
Revised: January 26, 2019
Published: February 5, 2019

DOI: 10.1021/acssuschemeng.8b06159
ACS Sustainable Chem. Eng. 2019, 7, 5240−5248

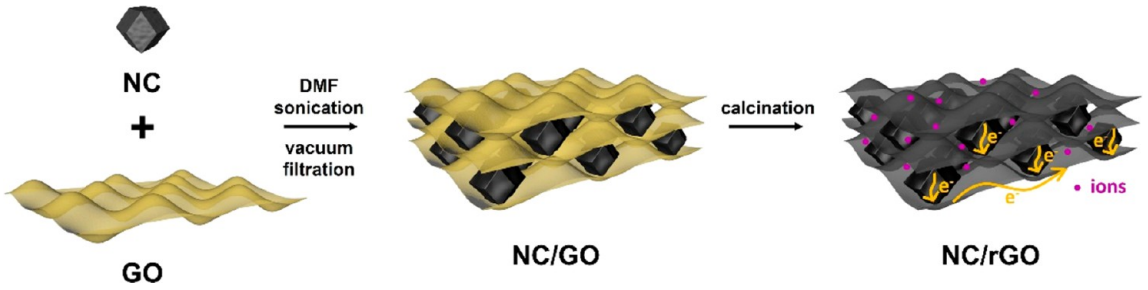

Figure 1. Schematic of the preparation of the NC/rGO nanopaper with efficient electron and ion transports.

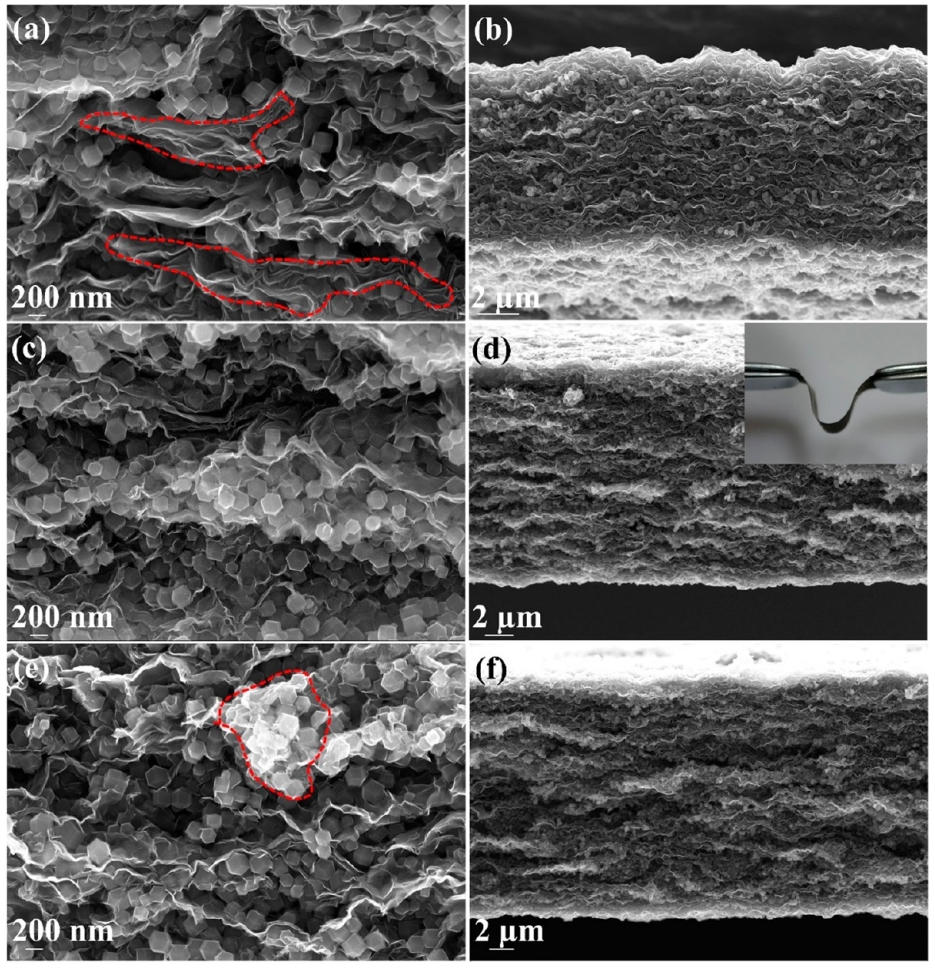

Figure 2. Cross section SEM images of (a, b) NC/rGO-1, (c, d) NC/rGO-2, and (e, f) NC/rGO-3 nanopapers. Insert of (d) shows high flexibility of NC/rGO-2 nanopaper.

decoration of ZIF8-derived carbon polyhedra on self-standing nanofiber membranes was successfully synthesized and used as electrodes for supercapacitors.[12,17,26,27] However, the preparation processes of these materials are complicated, and the loadings of carbon polyhedra within composite structures are relatively low. Therefore, the development of carbon polyhedra toward flexible electrodes for supercapacitors is highly desirable; however, it still represents a great challenge.

Herein, a nanopaper electrode consisting of N-doped carbon polyhedra (NC) and reduced graphene oxide (rGO) has been fabricated. The preparation of the NC/rGO nanopaper is pretty simple, and the as-obtained NC/rGO nanopaper can be directly used as a binder-free electrode for supercapacitors. In the NC/rGO nanopaper, the NC nanoparticles are uniformly decorated on rGO nanosheets, thus realizing complete exposures of active sites of the NC. Simultaneously, the presence of NC nanoparticles on the rGO surface effectively prevents the restacking of rGO, thus resulting in a unique interlayered framework. The hierarchical structure of NC/rGO nanopaper is beneficial for infiltration of electrolytic ions by shortening ion-diffusion distances. The rGO nanosheets not only bridge each individual NC nanoparticle by providing 3D electron-transfer pathway but also impart mechanical flexibility to the nanopaper. As a result, the resultant NC/rGO nanopaper performs with outstanding electrochemical performance of high specific capacitance, good rate performance, long cycling stability, and high energy density.

DOI: 10.1021/acssuschemeng.8b06159
ACS Sustainable Chem. Eng. 2019, 7, 5240−5248

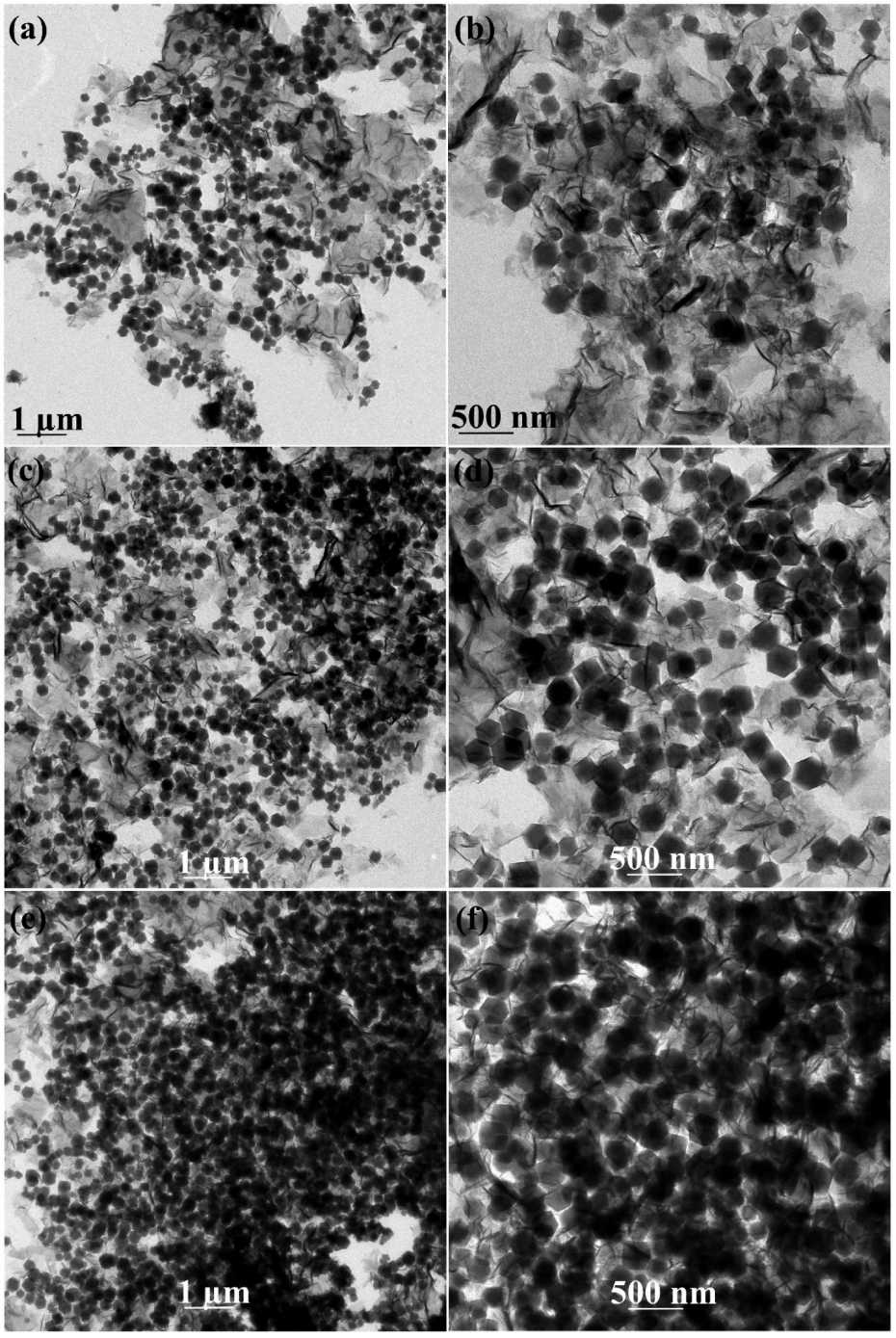

Figure 3. TEM images of (a, b) NC/rGO-1, (c, d) NC/rGO-2, and (e, f) NC/rGO-3 nanopapers.

RESULTS AND DISCUSSION

The as-prepared ZIF8 shows a well-defined polyhedron structure with particles sizes of ~200 nm (Figure S1). The ZIF8 was converted into the NC with a carbonization yield above 30 wt % by simple calcination under an inert atmosphere followed by acid leaching. The acid treatment removed residual Zn species within NC and simultaneously introduced oxygen-containing groups (hydroxyl, carboxyl, etc.), thus enhancing interfacial interactions between resultant NC and hydrophobic GO nanosheets. Figure S2 shows the morphology of NC nanoparticles with well-retained polyhedral shapes of slightly smaller size compared with the ZIF8. Transmission electron microscopy (TEM) images of NC (Figure S2c and d) indicate that the NC nanoparticles have a solid inside structure with numerous micro-/mesopores within the whole framework. Scanning transmission electron microscopy (STEM) image and corresponding elemental distribution mappings of NC (Figure S3) reveal that Zn metal centers in the ZIF8 have been successfully removed during pyrolysis, which is beneficial for improving ion adsorption/desorption performance by introducing additional porosities. Homogeneously dispersed C, N, and O elements within NC indicate a uniform doping of N atoms into NC, which dramatically improves the specific capacitances as well as the wettability of electrodes with ionic electrolytes.[28,29]

DOI: 10.1021/acssuschemeng.8b06159
ACS Sustainable Chem. Eng. 2019, 7, 5240−5248

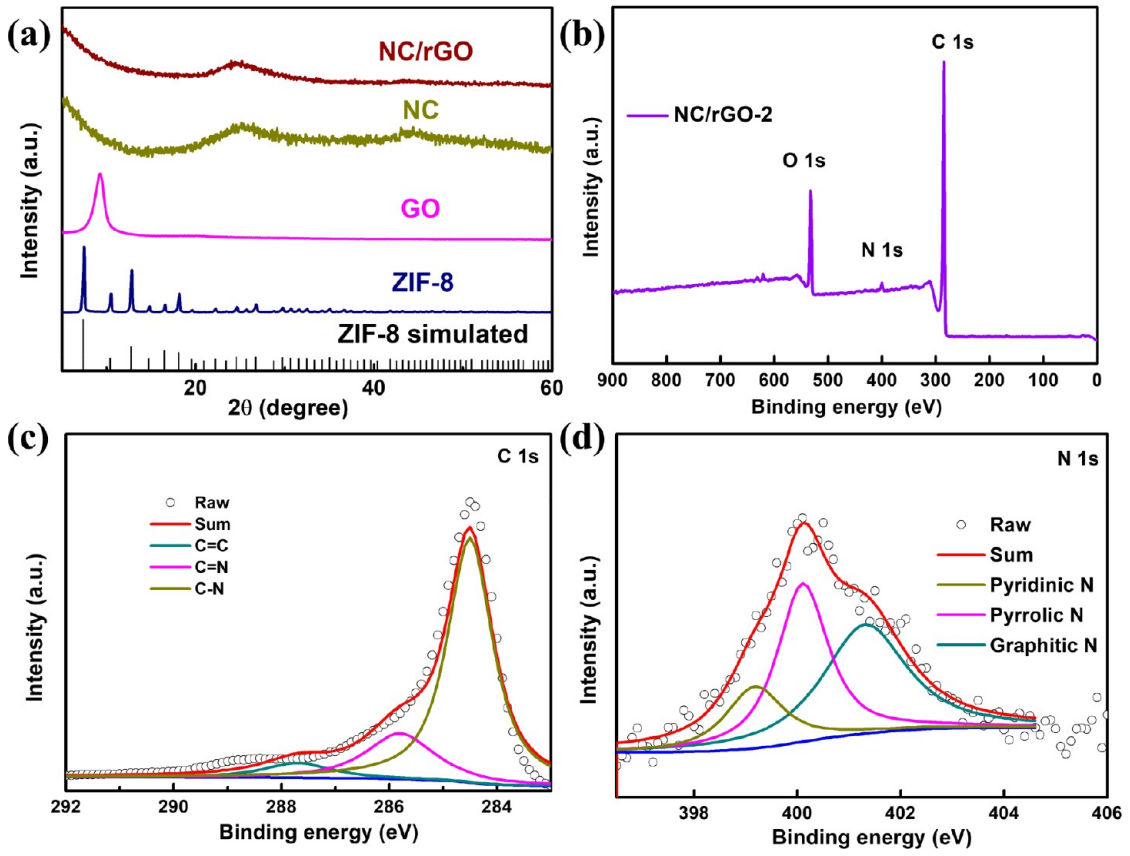

Figure 4. (a) XRD patterns of ZIF8, GO, NC, and NC/rGO. (b) XPS survey spectrum of NC/rGO. (c) C 1s and (d) N 1s XPS spectra of NC/rGO-2.

Figure 1 demonstrates the preparation process of NC/reduced GO (rGO) nanopaper. Scanning electron microscopy (SEM) and TEM images of as-prepared GO by modified Hummers' method are shown in Figure S4. The GO nanosheets with large lateral sizes (>30 μm) are selected for composition with NC, because large-size GO nanosheets are beneficial for achieving macroscopic assembly with high mechanical strengths.[30] The NC nanoparticles were mixed with GO in the *N*,*N*-dimethylformamide (DMF), and then the dispersion was vacuum-filtrated to form a nanopaper. After being peeled off from the filter, the NC/GO nanopaper was thermally reduced into NC/rGO nanopaper at 500 °C under an Ar atmosphere. The DMF was chosen as an optimized solvent because of its strong polarity beneficial for good dispersion of NC nanoparticles. For comparison, when deionized water was used as the solvent, the NC agglomerates formed even after sonication, and thus, a fragmentized nanopaper was obtained upon filtration. These results indicate that the dispersion solvent for the NC/GO hybrid has crucial effects on the formation of the NC/GO hybrid nanopaper.

The distribution of NC nanoparticles within the NC/GO nanopaper was monitored to further study the formation process of the hybrid nanopaper. Figures 2 and S5 are cross section and surface SEM images of the hybrid nanopapers with different loadings of NC. All the samples show a distinct interlayer structure with an oriented rGO framework. The NC nanoparticles are uniformly dispersed among rGO nanosheets in all samples. These results indicate that NC nanoparticles achieve an efficient contact with GO nanosheets under sonication. During filtration, the GO nanosheets stabilize the NC nanoparticles and suppress their intrinsic aggregations. Meanwhile, the NC nanoparticles between GO framework could prevent the restacking of GO nanosheets, thus forming a sandwiched structure. Upon themal reduction, the rGO framework endows the hybrid nanopaper with high mechanical flexibility (Figures 2d and S6), simplifying the utilization of carbon nanopaper as a flexible electrode. Besides, the NC/rGO nanopaper also shows relatively good mechanical stability, which remains stable after being bent for 100 cycles. When the content of NC within the nanopaper increases, the number of NC nanoparticles between rGO interlayers significantly increases, and the thickness of the nanopaper increases accordingly. The thicknesses of the NC/rGO-1, NC/rGO-2, and NC/rGO-3 nanopapers are estimated at about 10, 15, and 20 μm, respectively. When the nanopaper has a relatively large thickness, the infiltration of electrolytic ions inside the electrode matrix becomes difficult. In addition, some NC agglomerates are observed in the hybrid nanopaper when there is a high content of NC for the NC/rGO-3 sample (Figure 2e). Both factors have negative impacts on the resultant electrochemical performance of nanopaper samples as a self-standing electrode.

TEM characterizations were conducted to observe the formation of the NC/GO hybrid. For Figure 3, the NC nanoparticles are evenly anchored on the surface of GO in the whole view. No NC nanoparticles are observed independently located without the contact of GO nanosheets, indicating a strong interaction between NC and GO. The intimate contacts between NC and GO as well as rGO facilitate rapid electron transfer between individual NC nanoparticles, greatly improv-

DOI: 10.1021/acssuschemeng.8b06159
ACS Sustainable Chem. Eng. 2019, 7, 5240−5248

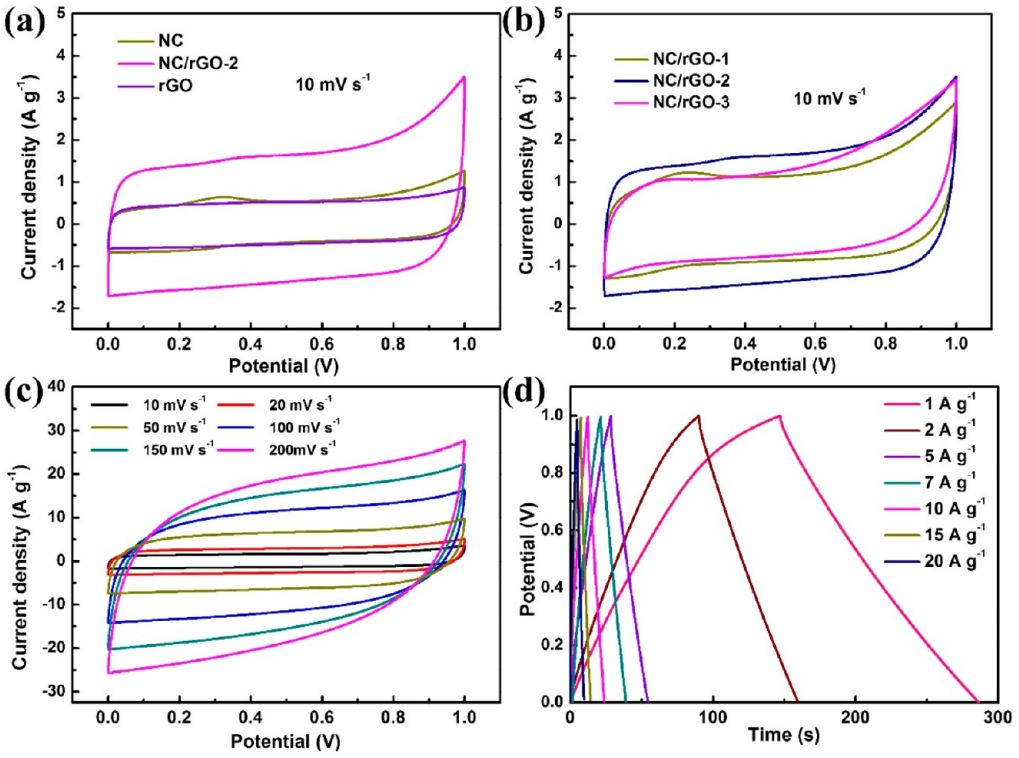

Figure 5. (a) CV curves of NC, NC/rGO-2, and rGO nanopaper electrodes at 10 mV s^{-1}. (b) CV curves of NC/rGO-1, NC/rGO-2, and NC/rGO-3 nanopaper electrodes at 10 mV s^{-1}. (c) CV curves of NC/rGO-2 nanopaper electrode at different scan rates. (d) Galvanostatic charge/discharge curves of NC/rGO-2 nanopaper electrode at different current densities.

ing the electrical conductivity of the nanopaper electrode. No curling or severe restacking of GO are observed, meaning that the NC components play a key role in suppressing the restacking of GO and rGO. When the content of NC within the NC/rGO hybrid nanopaper increases, the density of the NC nanoparticles on the surface of rGO increases accordingly. Even if the content of NC within the hybrid nanopaper increases to 50 wt %, NC nanoparticles maintain a uniform distribution within the rGO framework.

Figure 4a shows XRD patterns of GO, ZIF8, NC, and NC/rGO. The diffraction pattern at $2\theta = 9.3°$ of GO is ascribed to the (002) plane. The characteristic diffraction patterns of ZIF8 disappear upon pyrolysis, and only two broad patterns at $2\theta = 25°$ and 45° exist, revealing the successful conversion from ZIF8 to graphitic carbon materials. The NC/rGO shows similar patterns to NC, indicating the existence of NC components within the nanopaper. Compared with NC/GO, the I_D/I_G ratio (Raman spectra) of NC/rGO indicates that GO is successfully reduced after thermal reduction (Figure S7). XPS survey spectra (Figure 4b) further confirm the existence of N elements and the removal of Zn elements within the NC/rGO nanopaper, consistent with STEM-EDX (EDX = energy-dispersive X-ray spectroscopy) results. The contents of C, N, and O elements within the NC/rGO-2 nanopaper are 82.92, 2.35, and 14.73 at%, respectively. High-resolution C 1s XPS spectra of NC/rGO-2 (Figure 4c) reveal the presence of C═N and C−N bonds, indicating the N atoms are successfully doped into graphitic carbon lattices. The specific N configrations in NC/rGO are revealed by high-resolution N 1s XPS spectra (Figure 4d), namely, pyridinic N (398.7 eV), pyrrolic N (400.0 eV), and graphitic N (401.3 eV), respectively. XPS spectra of control samples are shown in Figure S8. The pore structures of as-prepared NC/rGO and NC were further studied by nitrogen adsorption/desorption measurements (Figure S9). The isotherms of NC/rGO-2 exhibit a combination of type I and IV isotherms, indicating the coexistence of micropores and mesopores.[31,32] The Brunauer−Emmett−Teller (BET) surface areas, total pore volumes, and half pore widths of related samples were tested and are summarized in Table S1. The pore size distributions of NC/rGO calculated by Barrett−Joyner−Halenda (BJH) method (Figure S9b) reveal that the NC/rGO nanopapers possess broad pore distributions, thus achieving efficient ion infiltrations.

The electrochemical performances of NC, NC/rGO-1, NC/rGO-2, NC/rGO-3, and rGO were evaluated by assembly of two nanopaper samples sandwiched with filter paper separator via two-electrode configuration in 6 M KOH electrolyte. Cyclic voltammogram (CV) curves of the NC, NC/rGO, and rGO nanopaper electrodes were collected in the potential range of 0−1 V at a scan rate of 10 mV s^{-1}. Figure 5a exhibits that all CV curves display nearly rectangular shapes, indicating ideal electric double layer capacitance behaviors. The weak peaks in the CV curves of NC and NC/rGO samples correspond to pseudocapacitive behaviors due to N-doping. CV curve of the NC/rGO-2 electrode exhibits a much larger area than that of neat NC and rGO electrodes, indicating that the NC/rGO-2 electrode stores the highest capacitances among these samples. This is because, in neat NC electrode, the NC nanoparticles are easily agglomerated, making electrolytic ions difficult to diffuse into the interior parts of the electrode matrix, thus greatly reducing the amounts of electrochemically active sites of NC. In addition, the lack of efficient conductive pathways between individual NC nanoparticles makes the electron transfers inside the electrode matrix not that efficient. In neat rGO nanopaper, rGO nanosheets stack into a compact

DOI: 10.1021/acssuschemeng.8b06159
ACS Sustainable Chem. Eng. 2019, 7, 5240−5248

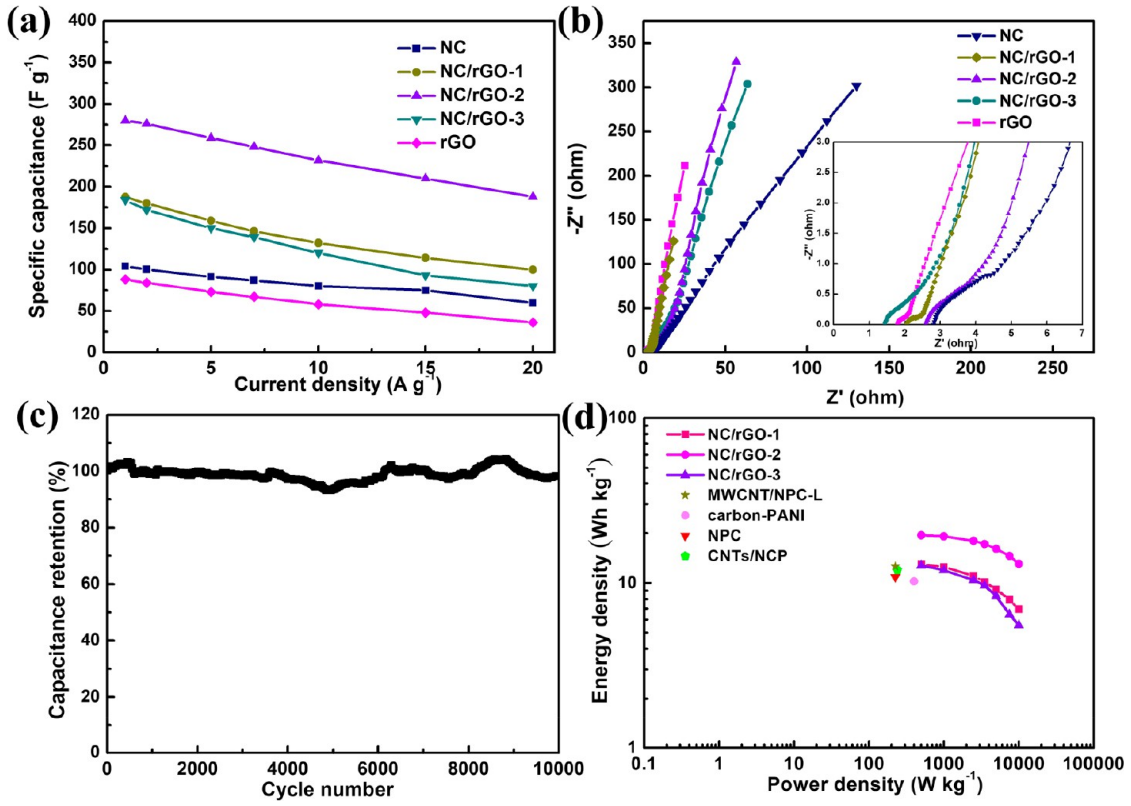

Figure 6. (a) Rate performance and (b) Nyquist plots of NC, NC/rGO-1, NC/rGO-2, NC/rGO-3, and rGO nanopaper electrodes. (c) Long-term stability of NC/rGO-2 nanopaper electrode at 5 A g^{-1}. (d) Ragone plots of supercapacitors using the NC/rGO nanopaper electrodes.

assembled structure under vacuum filtration. The compact structure hinders infiltrations of electrolytic ions, leading to an insufficient utilization of the intrinsic high surface area of rGO.[33,34] In the NC/rGO hybrid nanopaper, well-distributed NC nanoparticles fully expose active sites, and the rGO framework bridges each NC nanoparticle into an interconnected conductive pathway, ensuring fast electron transfer inside the electrode matrix, thus obtaining high specific capacitances and excellent rate performance.[35]

Figure 5b shows CV curves of NC/rGO electrodes at the scan rate of 10 mV s^{-1}, indicating the NC/rGO-2 electrode has the highest specific capacitance. This is because the ion absorption/desorption on the surface of electrode materials provides efficient capacitances, and obviously porous structures of electrodes would have great influences on their final capacitive performance. The NC content within the NC/rGO-1 is relatively low, and therefore there exist some densely packed rGO nanosheets (highlighted by red lines in Figure 2a), resulting in relatively low porosity and small specific capacitance. The NC content within NC/rGO-3 is too high, and rGO nanosheets could not afford enough surfaces for anchoring NC nanoparticles. Hence, excessive NC nanoparticles form severe aggregations (highlighted by red lines in Figure 2e) and cause the decrease of capacitances. CV curves of the NC/rGO-2 electrode under different scan rates are shown in Figure 5c. The areas of the CV curves increase with the increase of scan rates, and the CV curves remain nearly rectangular shapes with slight distortions even at a high scan rate up to 200 mV s^{-1}, indicating an outstanding rate performance.[27] The superior capacitive performance of the NC/rGO-2 electrode was further measured by galvanostatic charge/discharge tests under different current densities (Figure 5d). All the curves display symmetric linear shapes, revealing good capacitive performance. The NC/rGO-2 electrode exhibits a very low *iR* drop during the discharge processes, implying low internal resistance and high columbic efficiency. For comparison, detailed CV and galvanostatic charge/discharge curves of NC/rGO-1 and NC/rGO-3 can be found in Figure S10.

Comparisons of specific capacitances of different samples under different current densities that are calculated from the discharge profiles are shown in Figure 6a. All the NC/rGO electrodes have much larger specific capacitances than that of neat NC and rGO electrodes under the measured current densities, consistent with previous CV results. Specifically, the NC/rGO-2 electrode delivers high specific capacitance of 280 F g^{-1} at the current density of 1 A g^{-1}, which is much higher than those of NC/rGO-1 (188 F g^{-1}), NC/rGO-3 (184 F g^{-1}), NC (104 F g^{-1}), and rGO (88 F g^{-1}). Meanwhile, the NC/rGO-2 electrode retains a high specific capacitance of 188 F g^{-1} when the current density increases to 20 A g^{-1}, corresponding to the high capacitance retention of 67% with excellent rate performance. Meanwhile, the NC and rGO electrodes only have a specific capacitance of 60 and 36 F g^{-1}, respectively, at the current density of 20 A g^{-1}. The outstanding rate performance of NC/rGO-2 is derived from its integrated conductive pathways and rational pore structures. The abundant micro-/mesopores and sandwiched structures together enhance the electrolyte infiltration and greatly shorten ion-diffusion distances, thus realizing rapid charge accumulations of the whole electrode.

Electrochemical impedance spectroscopy (EIS) measurements were carried out under an open-circuit potential to investigate internal resistances and charge-transfer kinetics of

DOI: 10.1021/acssuschemeng.8b06159
ACS Sustainable Chem. Eng. 2019, 7, 5240−5248

Table 1. Comparison of Supercapacitors Using NC/rGO Nanopaper Electrodes with Other ZIF8-Derived Electrodes in the Literature

electrode material	specific capacitance [F g^{-1}]	device configuration	status of electrode materials	energy density [W h kg^{-1}]	ref
C-GZ	238 at 1 A g^{-1}	two-electrode	aerogel		40
MWCNT/NPC-L	112.4 at 0.5 A g^{-1}	two-electrode	powder	12.65	37
3D hybrid-porous carbon	332 at 0.5 A g^{-1}	three-electrode	powder		41
CNT@CZIF	324 at 0.5 A g^{-1}	three-electrode	powder		42
S-900	56.6 at 0.1 A g^{-1}	two-electrode	powder	6.44 mWh cm^{-3}	43
PC1000@C	225 at 0.5 A g^{-1}	three-electrode	powder		44
NHCFs	302 at 0.5 A g^{-1}	three-electrode	nanopaper		26
nanoporous carbon	20 at 1 A g^{-1}	two-electrode	powder	7.1	45
NPCF	332 at 1 A g^{-1}	three-electrode	nanopaper		17
HPCNFs-N	307.2 at 1.0 A g^{-1}	two-electrode	nanopaper	10.96	46
NC	239 at 2 A g^{-1}	three-electrode	powder		47
AS-ZC-800	211 at 10 mV s^{-1}	two-electrode	powder		48
NPC	251 at 5 mV s^{-1}	two-electrode	powder	10.86	39
NC800-PEDOT	217.7 at 5 mV s^{-1}	three-electrode	powder		49
NCGs	225 at 0.5 A g^{-1}	two-electrode	powder	12.7	50
NC/rGO	280 at 1 A g^{-1}	two-electrode	nanopaper	19.45	this work

electrodes. The sloping lines at low-frequency regions in Figure 6b reflect the mass-transfer processes of electrodes. A larger slope indicates a faster ion-diffusion rate inside the electrode.[36] Among the samples, the NC electrode shows the slowest ion-diffusion rate due to aggregations of NC nanoparticles. The introduction of rGO nanosheets into the NC matrix increases the ion-diffusion rate because rGO nanosheets help to expose more NC nanoparticles with shortened ion-diffusion distances. From the inset of Figure 6b, the rGO and NC electrodes have the lowest and highest charge-transfer resistances (R_{ct}), respectively. As the rGO contents increase in the NC/rGO samples, the R_{ct} of NC/rGO gradually decreases, implying rGO nanosheets as efficient conductive pathways inside the electrode.

Long-term cycling stability is a vital evaluation criterion for supercapacitors in practical applications. The NC/rGO-2 electrode remains stable after >10 000 cycles (Figure 6c), exhibiting excellent long-term stability. Figure 6d shows Ragone plots by giving a comparison of the energy density and power density of supercapacitors with our NC/rGO nanopaper electrodes and other ZIF8-derived carbon materials. The energy density of the as-assemblied supercapacitor device is 19.45 W h kg^{-1} at a power density of 500 W kg^{-1}. When the power density increases to 5 000 W kg^{-1}, the supercapacitor device still delivers a high energy density of 16.1 W h kg^{-1}, surpassing most of the supercapacitor devices using other ZIF8-derived carbon materials in the literature.[13,37−42] Comparisons of the electrochemical performance and other parameters between this study and other ZIF8-related electrodes in the literature are summarized in Table 1. Considering the convenient device assembly of nanopaper electrodes and easy preparation for NC/rGO nanopaper, this study therefore provides a simple and convenient way for development of promising electrode materials for supercapacitors.

On the basis of the earlier discussions, the possible mechanism of excellent performance of NC/rGO nanopaper electrodes for supercapacitors is proposed. First, uniformly dispersed NC nanoparticles have numerous micropores and mesopores, which provide abundant active sites for charge accumulations. Second, highly conductive rGO nanosheets bridge individual NC nanoparticles, ensuring fast electron transfers inside the whole electrode and simultaneously endowing the nanopaper with excellent mechanical flexibility. Third, hierarchical porous structures of the NC/rGO shorten the diffusion distance and thus allow fast ion transports during rapid charge/discharge processes. All these advantages contribute to improving the electrochemical performance and thus helping to obtain excellent electrochemical energy storage performance of the NC/rGO nanopaper electrodes.

CONCLUSION

In summary, a flexible nanopaper electrode consisting of ZIF8-derived N-doped porous carbon polyhedra (NC) and reduced graphene oxide (rGO) has been prepared. The as-obtained NC/rGO nanopaper shows good mechanical flexibility, which is directly used as a binder-free electrode for symmetric supercapacitors. Benefiting from hierarchical structure, high conductivity, and good chemical stability, the NC/rGO nanopaper electrode delivers high specific capacitance of 280 F g^{-1} at 1 A g^{-1}, good rate capacitance, high energy density, and high capacitance retention over 10 000 cycles. This work therefore provides new insights for rational design and construction of flexible MOF-derived carbon electrodes for high-performance supercapacitors.

ASSOCIATED CONTENT

Supporting Information

The Supporting Information is available free of charge on the ACS Publications website at DOI: 10.1021/acssuschemeng.8b06159.

Materials, preparation of ZIF8, NC, NC/rGO nanopaper, characterization, electrochemical measurements, SEM images of ZIF-8, SEM and TEM images of NC, STEM image and EDX elemental mappings of NC, SEM and TEM images of GO, SEM images of NC/rGO-1, NC/rGO-2, and NC/rGO-3 nanopapers, NC/rGO-2 nanopaper under bending tests, Raman spectra of NC/GO and NC/rGO, XPS spectra and elements contents of rGO, NC/rGO-1, NC/rGO-3, and NC, nitrogen adsorption/desorption isotherms and pore size distribution of NC/rGO-2, CV and galvanostatic charge/discharge curves of NC/rGO-1 and NC/rGO-3, and a

DOI: 10.1021/acssuschemeng.8b06159
ACS Sustainable Chem. Eng. 2019, 7, 5240−5248

table summarizing BET surface areas and pore volumes of related samples (PDF)

AUTHOR INFORMATION

Corresponding Authors

*E-mail: czhang@dhu.edu.cn.
*E-mail: txliu@fudan.edu.cn or txliu@dhu.edu.cn.

ORCID

Chao Zhang: 0000-0003-1255-7183
Tianxi Liu: 0000-0002-5592-7386

Notes

The authors declare no competing financial interest.

ACKNOWLEDGMENTS

We are grateful for the financial support from the Fundamental Research Funds for the Central Universities (2232016A3-02), the National Natural Science Foundation of China (51433001, 21504012, and 51773035), the Program of Shanghai Academic Research Leader (17XD1400100), the Science and Technology Commission of Shanghai Municipality (16520722100), and the Shanghai Scientific and Technological Innovation Project (18JC1410600).

REFERENCES

(1) Zhang, W.; Wu, Z.; Jiang, H.; Yu, S. Nanowire-directed templating synthesis of metal−organic framework nanofibers and their derived porous doped carbon nanofibers for enhanced electrocatalysis. *J. Am. Chem. Soc.* **2014**, *136* (41), 14385−14388.

(2) Li, B.; Wen, H.; Cui, Y.; Zhou, W.; Qian, G.; Chen, B. Emerging multifunctional metal-organic framework materials. *Adv. Mater.* **2016**, *28* (40), 8819−8860.

(3) Wang, J.; Tang, J.; Ding, B.; Chang, Z.; Hao, X.; Takei, T.; Kobayashi, N.; Bando, Y.; Zhang, X.; Yamauchi, Y. Self-template-directed metal−organic frameworks network and the derived honeycomb-like carbon flakes via confinement pyrolysis. *Small* **2018**, *14* (14), 1704461.

(4) Kirchon, A.; Feng, L.; Drake, H. F.; Joseph, E. A.; Zhou, H. From fundamentals to applications: A toolbox for robust and multifunctional MOF materials. *Chem. Soc. Rev.* **2018**, *47* (23), 8611−8638.

(5) Zhang, P.; Guan, B. Y.; Yu, L.; Lou, X. W. D. Formation of double-shelled zinc−cobalt sulfide dodecahedral cages from bimetallic zeolitic imidazolate frameworks for hybrid supercapacitors. *Angew. Chem., Int. Ed.* **2017**, *56* (25), 7141−7145.

(6) Wang, L.; Han, Y.; Feng, X.; Zhou, J.; Qi, P.; Wang, B. Metal−organic frameworks for energy storage: Batteries and supercapacitors. *Coord. Chem. Rev.* **2016**, *307*, 361−381.

(7) Jeon, J.; Sharma, R.; Meduri, P.; Arey, B. W.; Schaef, H. T.; Lutkenhaus, J. L.; Lemmon, J. P.; Thallapally, P. K.; Nandasiri, M. I.; McGrail, B. P.; Nune, S. K. In situ one-step synthesis of hierarchical nitrogen-doped porous carbon for high-performance supercapacitors. *ACS Appl. Mater. Interfaces* **2014**, *6* (10), 7214−7222.

(8) Yi, F.; Zhang, R.; Wang, H.; Chen, L.; Han, L.; Jiang, H.; Xu, Q. Metal−organic frameworks and their composites: Synthesis and electrochemical applications. *Small Methods* **2017**, *1* (11), 1700187.

(9) Zhu, K.; Chen, C.; Xu, H.; Gao, Y.; Tan, X.; Alsaedi, A.; Hayat, T. Cr(VI) reduction and immobilization by core-double-shell structured magnetic polydopamine@zeolitic idazolate frameworks-8 microspheres. *ACS Sustainable Chem. Eng.* **2017**, *5* (8), 6795−6802.

(10) Chaikittisilp, W.; Hu, M.; Wang, H.; Huang, H.; Fujita, T.; Wu, K. C. W.; Chen, L.; Yamauchi, Y.; Ariga, K. Nanoporous carbons through direct carbonization of a zeolitic imidazolate framework for supercapacitor electrodes. *Chem. Commun.* **2012**, *48* (58), 7259−7261.

(11) Tang, Z.; Zhang, G.; Zhang, H.; Wang, L.; Shi, H.; Wei, D.; Duan, H. MOF-derived N-doped carbon bubbles on carbon tube arrays for flexible high-rate supercapacitors. *Energy Storage Mater.* **2018**, *10*, 75−84.

(12) Wang, C.; Kaneti, Y. V.; Bando, Y.; Lin, J.; Liu, C.; Li, J.; Yamauchi, Y. Metal−organic framework-derived one-dimensional porous or hollow carbon-based nanofibers for energy storage and conversion. *Mater. Horiz.* **2018**, *5* (3), 394−407.

(13) Xu, X.; Wang, M.; Liu, Y.; Li, Y.; Lu, T.; Pan, L. In situ construction of carbon nanotubes/nitrogen-doped carbon polyhedra hybrids for supercapacitors. *Energy Storage Mater.* **2016**, *5*, 132−138.

(14) Wan, L.; Shamsaei, E.; Easton, C. D.; Yu, D.; Liang, Y.; Chen, X.; Abbasi, Z.; Akbari, A.; Zhang, X.; Wang, H. ZIF-8 derived nitrogen-doped porous carbon/carbon nanotube composite for high-performance supercapacitor. *Carbon* **2017**, *121*, 330−336.

(15) Liu, Y.; Li, G.; Guo, Y.; Ying, Y.; Peng, X. Flexible and binder-free hierarchical porous carbon film for supercapacitor electrodes derived from MOFs/CNT. *ACS Appl. Mater. Interfaces* **2017**, *9* (16), 14043−14050.

(16) Sumboja, A.; Liu, J.; Zheng, W. G.; Zong, Y.; Zhang, H.; Liu, Z. Electrochemical energy storage devices for wearable technology: A rationale for materials selection and cell design. *Chem. Soc. Rev.* **2018**, *47* (15), 5919−5945.

(17) Wang, C.; Liu, C.; Li, J.; Sun, X.; Shen, J.; Han, W.; Wang, L. Electrospun metal−organic framework derived hierarchical carbon nanofibers with high performance for supercapacitors. *Chem. Commun.* **2017**, *53* (10), 1751−1754.

(18) Peng, L.; Zhu, Y.; Li, H.; Yu, G. Chemically integrated inorganic-graphene two-dimensional hybrid materials for flexible energy storage devices. *Small* **2016**, *12* (45), 6183−6199.

(19) Yuan, C.; Yang, L.; Hou, L.; Li, J.; Sun, Y.; Zhang, X.; Shen, L.; Lu, X.; Xiong, S.; Lou, X. W. D. Flexible hybrid paper made of monolayer Co3O4 microsphere arrays On RGO/CNTs and their application in electrochemical capacitors. *Adv. Funct. Mater.* **2012**, *22* (12), 2560−2566.

(20) Zheng, Q.; Kvit, A.; Cai, Z.; Ma, Z.; Gong, S. A freestanding cellulose nanofibril−reduced graphene oxide−molybdenum oxynitride aerogel film electrode for all-solid-state supercapacitors with ultrahigh energy density. *J. Mater. Chem. A* **2017**, *5* (24), 12528−12541.

(21) Choudhury, A.; Kim, J.; Sinha Mahapatra, S.; Yang, K.; Yang, D. Nitrogen-enriched porous carbon nanofiber mat as efficient flexible electrode material for supercapacitors. *ACS Sustainable Chem. Eng.* **2017**, *5* (3), 2109−2118.

(22) Sun, K.; Feng, E.; Zhao, G.; Peng, H.; Wei, G.; Lv, Y.; Ma, G. A single robust hydrogel film based integrated flexible supercapacitor. *ACS Sustainable Chem. Eng.* **2019**, *7* (1), 165−173.

(23) Huang, Z.; Li, L.; Wang, Y.; Zhang, C.; Liu, T. Polyaniline/graphene nanocomposites towards high-performance supercapacitors: A review. *Compos. Commun.* **2018**, *8*, 83−91.

(24) Wan, C.; Jiao, Y.; Li, J. Flexible, highly conductive, and free-standing reduced graphene oxide/polypyrrole/cellulose hybrid papers for supercapacitor electrodes. *J. Mater. Chem. A* **2017**, *5* (8), 3819−3831.

(25) Liu, J.; Zhang, L.; Wu, H. B.; Lin, J.; Shen, Z.; Lou, X. W. D. High-performance flexible asymmetric supercapacitors based on a new graphene foam/carbon nanotube hybrid film. *Energy Environ. Sci.* **2014**, *7* (11), 3709−3719.

(26) Yao, Y.; Wu, H.; Huang, L.; Li, X.; Yu, L.; Zeng, S.; Zeng, X.; Yang, J.; Zou, J. Nitrogen-enriched hierarchically porous carbon nanofiber network as a binder-free electrode for high-performance supercapacitors. *Electrochim. Acta* **2017**, *246*, 606−614.

(27) Guo, C. X.; Li, C. M. A Self-assembled hierarchical nanostructure comprising carbon spheres and graphene nanosheets for enhanced supercapacitor performance. *Energy Environ. Sci.* **2011**, *4* (11), 4504−4507.

(28) Lee, W. J.; Maiti, U. N.; Lee, J. M.; Lim, J.; Han, T. H.; Kim, S. O. Nitrogen-doped carbon nanotubes and graphene composite

DOI: 10.1021/acssuschemeng.8b06159
ACS Sustainable Chem. Eng. 2019, 7, 5240−5248

structures for energy and catalytic applications. *Chem. Commun.* **2014**, *50* (52), 6818−6830.
(29) Yan, L.; Li, D.; Yan, T.; Chen, G.; Shi, L.; An, Z.; Zhang, D. N,P,S-codoped hierarchically porous carbon spheres with well-balanced gravimetric/volumetric capacitance for supercapacitors. *ACS Sustainable Chem. Eng.* **2018**, *6* (4), 5265−5272.
(30) Xu, Z.; Sun, H.; Zhao, X.; Gao, C. Ultrastrong fibers assembled from giant graphene oxide sheets. *Adv. Mater.* **2013**, *25* (2), 188−193.
(31) Munn, A. S.; Dunne, P. W.; Tang, S. V. Y.; Lester, E. H. Large-scale continuous hydrothermal production and activation of ZIF-8. *Chem. Commun.* **2015**, *51* (64), 12811−12814.
(32) Niu, J.; Liang, J.; Shao, R.; Liu, M.; Dou, M.; Li, Z.; Huang, Y.; Wang, F. Tremella-like N,O-codoped hierarchically porous carbon nanosheets as high-performance anode materials for high energy and ultrafast Na-ion capacitors. *Nano Energy* **2017**, *41*, 285−292.
(33) Jiang, L.; Sheng, L.; Long, C.; Fan, Z. Densely packed graphene nanomesh-carbon nanotube hybrid film for ultra-high volumetric performance supercapacitors. *Nano Energy* **2015**, *11*, 471−480.
(34) Fan, Z.; Yan, J.; Zhi, L.; Zhang, Q.; Wei, T.; Feng, J.; Zhang, M.; Qian, W.; Wei, F. A three-dimensional carbon nanotube/graphene sandwich and its application as electrode in supercapacitors. *Adv. Mater.* **2010**, *22* (33), 3723−3728.
(35) Wang, L.; Wei, T.; Sheng, L.; Jiang, L.; Wu, X.; Zhou, Q.; Yuan, B.; Yue, J.; Liu, Z.; Fan, Z. Brick-and-mortar" sandwiched porous carbon building constructed by metal-organic framework and graphene: Ultrafast charge/discharge rate up to 2 V s^{-1} for supercapacitors. *Nano Energy* **2016**, *30*, 84−92.
(36) Zhao, Z.; Liu, S.; Zhu, J.; Xu, J.; Li, L.; Huang, Z.; Zhang, C.; Liu, T. Hierarchical nanostructures of nitrogen-doped porous carbon polyhedrons confined in carbon nanosheets for high-performance supercapacitors. *ACS Appl. Mater. Interfaces* **2018**, *10* (23), 19871−19880.
(37) Li, X.; Hao, C.; Tang, B.; Wang, Y.; Liu, M.; Wang, Y.; Zhu, Y.; Lu, C.; Tang, Z. Supercapacitor electrode materials with hierarchically structured pores from carbonization of MWCNTs and ZIF-8 composites. *Nanoscale* **2017**, *9* (6), 2178−2187.
(38) Salunkhe, R. R.; Tang, J.; Kobayashi, N.; Kim, J.; Ide, Y.; Tominaka, S.; Kim, J. H.; Yamauchi, Y. Ultrahigh performance supercapacitors utilizing core−shell nanoarchitectures from a metal−organic framework-derived nanoporous carbon and a conducting polymer. *Chem. Sci.* **2016**, *7* (9), 5704−5713.
(39) Salunkhe, R. R.; Kamachi, Y.; Torad, N. L.; Hwang, S. M.; Sun, Z.; Dou, S. X.; Kim, J. H.; Yamauchi, Y. Fabrication of symmetric supercapacitors based on MOF-derived nanoporous carbons. *J. Mater. Chem. A* **2014**, *2* (46), 19848−19854.
(40) Li, C.; Hu, C.; Zhao, Y.; Song, L.; Zhang, J.; Huang, R.; Qu, L. Decoration of graphene network with metal−organic frameworks for enhanced electrochemical capacitive behavior. *Carbon* **2014**, *78*, 231−242.
(41) Bao, W.; Mondal, A. K.; Xu, J.; Wang, C.; Su, D.; Wang, G. 3D hybrid−porous carbon derived from carbonization of metal organic frameworks for high performance supercapacitors. *J. Power Sources* **2016**, *325*, 286−291.
(42) Wan, L.; Shamsaei, E.; Easton, C. D.; Yu, D.; Liang, Y.; Chen, X.; Abbasi, Z.; Akbari, A.; Zhang, X.; Wang, H. ZIF-8 derived nitrogen-doped porous carbon/carbon nanotube composite for high-performance supercapacitor. *Carbon* **2017**, *121*, 330−336.
(43) Young, C.; Salunkhe, R. R.; Tang, J.; Hu, C.; Shahabuddin, M.; Yanmaz, E.; Hossain, M. S. A.; Kim, J. H.; Yamauchi, Y. Zeolitic imidazolate framework (ZIF-8) derived nanoporous carbon: The effect of carbonization temperature on the supercapacitor performance in an aqueous electrolyte. *Phys. Chem. Chem. Phys.* **2016**, *18* (42), 29308−29315.
(44) Jiang, M.; Cao, X.; Zhu, D.; Duan, Y.; Zhang, J. Hierarchically porous N-doped carbon derived from ZIF-8 nanocomposites for electrochemical applications. *Electrochim. Acta* **2016**, *196*, 699−707.
(45) Salunkhe, R. R.; Tang, J.; Kamachi, Y.; Nakato, T.; Kim, J. H.; Yamauchi, Y. Asymmetric supercapacitors using 3D nanoporous carbon and cobalt oxide electrodes synthesized from a single metal−organic framework. *ACS Nano* **2015**, *9* (6), 6288−6296.
(46) Chen, L.; Lu, Y.; Yu, L.; Lou, X. W. D. Designed formation of hollow particle-based nitrogen-doped carbon nanofibers for high-performance supercapacitors. *Energy Environ. Sci.* **2017**, *10* (8), 1777−1783.
(47) Tang, J.; Salunkhe, R. R.; Liu, J.; Torad, N. L.; Imura, M.; Furukawa, S.; Yamauchi, Y. Thermal conversion of core−shell metal−organic frameworks: A new method for selectively functionalized nanoporous hybrid carbon. *J. Am. Chem. Soc.* **2015**, *137* (4), 1572−1580.
(48) Amali, A. J.; Sun, J.; Xu, Q. From assembled metal-organic framework nanoparticles to hierarchically porous carbon for electrochemical energy storage. *Chem. Commun.* **2014**, *50* (13), 1519−1522.
(49) Li, Y.; Kim, J.; Wang, J.; Liu, N.; Bando, Y.; Alshehri, A. A.; Yamauchi, Y.; Hou, C.; Wu, K. C. W. High performance capacitive deionization using modified ZIF-8-derived, N-doped porous carbon with improved conductivity. *Nanoscale* **2018**, *10* (31), 14852−14859.
(50) Wang, L.; Wang, C.; Wang, H.; Jiao, X.; Ouyang, Y.; Xia, X.; Lei, W.; Hao, Q. ZIF-8 nanocrystals derived N-doped carbon decorated graphene sheets for symmetric supercapacitors. *Electrochim. Acta* **2018**, *289*, 494−502.

DOI: 10.1021/acssuschemeng.8b06159
ACS Sustainable Chem. Eng. 2019, 7, 5240−5248